Energy 66 (2014) 598–609

Contents lists available at ScienceDirect

Energy

journal homepage: www.elsevier.com/locate/energy

Buildings roofs photovoltaic potential assessment based on LiDAR (Light Detection And Ranging) data

Niko Lukač [a,c,*], Sebastijan Seme [b], Danijel Žlaus [a,c], Gorazd Štumberger [a,d], Borut Žalik [a,c]

[a] University of Maribor, Faculty of Electrical Engineering and Computer Science, Smetanova ulica 17, SI-2000 Maribor, Slovenia
[b] University of Maribor, Faculty of Energy Technology, Hočevarjev trg 1, SI-8270 Krško, Slovenia
[c] Laboratory for Geometric Modeling and Multimedia Algorithms, Slovenia
[d] Power Engineering Laboratory, Slovenia

ARTICLE INFO

Article history:
Received 13 June 2013
Received in revised form
25 December 2013
Accepted 28 December 2013
Available online 26 January 2014

Keywords:
Solar energy
Photovoltaic potential
Photovoltaic systems
LiDAR (Light Detection And Ranging) data

ABSTRACT

One of the major challenges today is assessing the suitability of PV (photovoltaic) systems' installations on buildings' roofs regarding the received solar irradiance. The availability of aerial laser-scanning, namely LiDAR (Light Detection And Ranging), means that assessment can be performed automatically over large-scale urban areas in high accuracy by considering surfaces' topographies, long-term direct and diffuse irradiance measurements, and influences of shadowing. The solar potential metric was introduced for this purpose, however it fails to provide any insights into the production of electrical energy by a specific PV system. Hence, the PV potential metric can be used that integrates received instantaneous irradiance which is then multiplied by the PV system's efficiency characteristics. Many existing PV potential metrics over LiDAR data consider the PV modules' efficiencies to be constant, when in reality they are nonlinear. This paper presents a novel PV potential estimation over LiDAR data, where the PV modules' and solar inverter's nonlinear efficiency characteristics are approximated by modelled functions. The estimated electrical energy production from buildings' roofs within an urban area was extensively analysed by comparing the constant and nonlinear efficiency characteristics of different PV module types and solar inverters. The obtained results were confirmed through measurements performed on an existing PV system.

1. Introduction

Solar energy is one of the more promising and sustainable energy sources due to its good accessibility. Over recent years, the technology that uses the PV (photovoltaic) effect for the production of electrical power has progressed immensely [1]. Various parameters have to be considered when installing grid-connected PV systems [2,3], as some buildings' roofs are more suitable than others, regarding the received solar irradiance. This presents an important issue in urban planning and the environmental health of modern sustainable cities. The solar potential (i.e. average daily or total received irradiance on a given surface throughout the year) is one of the more reliable metrics for finding the most suitable surfaces for PV systems' installations. Some of the more important parameters to be considered in solar potential estimation are: geographic location, surface topography, influence of atmospheric attenuation by molecular absorption and Rayleigh or Mie scattering, and shadowing effects from the surroundings. The estimation of solar irradiance (i.e. irradiation incident on surface) provides a direct solution for calculating the solar potential. Accurate methods split the global irradiance into direct and diffuse irradiances, which is possible with solar radiation modelling [4–24], or by using long-term shortwave global and diffuse irradiance measurements (e.g. with a pyranometer) near the considered location. The diffuse irradiance is the consequence of various perturbations of the direct irradiance (e.g. atmospheric attenuation, cloud cover and air pollution), and unlike direct irradiance it also irradiates any shadowed areas that are only partly obstructed from their surroundings. The solar irradiance models based on measured data are mainly differentiated by whether the diffuse irradiance is estimated as isotropic or more accurately as anisotropic. Demain et al. [17] compared the well-established models, and concluded that Bugler's [4], Willmot's [5], and Perez's [6] model performed best under clear sky, partially-cloudy sky, and overcast conditions, respectively. Irradiance can also be estimated from newer satellites' measurements of irradiance spectra

* Corresponding author. University of Maribor, Faculty of Electrical Engineering and Computer Science, Smetanova ulica 17, SI-2000 Maribor, Slovenia. Tel.: +386 2 220 7435; fax: +386 2 220 7272.
E-mail addresses: niko.lukac@um.si, niko.lukac@gmail.com (N. Lukač).

0360-5442/$ – see front matter © 2014 Elsevier Ltd. All rights reserved.
http://dx.doi.org/10.1016/j.energy.2013.12.066

[7,12,23]. Although on-site measurements are in higher resolution, the satellite spectra have a distinct advantage in a few cases, e.g. observing mountainous terrain, where few on-site irradiance-monitoring stations exist and their interpolations yield less accurate estimations. Alternatively a less accurate irradiance can be derived from other geophysical variables [24] such as temperature, rainfall, and sunshine duration.

LiDAR (Light Detection And Ranging) is an active remote sensing technology [25] that captures surfaces topographies in high detail, which can be used for accurate automatic solar irradiance estimations over large-scale urban areas [8]. The scanning is done by emitting laser pulses between ca. 10 nm–250 nm wavelengths. The result of such scanning is an unstructured 3D point cloud consisting of millions of unclassified points. Over the past few years various methods have been developed for estimating solar potential by considering remote sensing data [26–47], where most originate from ALS (Airborne Laser Scanning). Most commonly, the classified LiDAR point cloud is geo-referenced (e.g. with a Global Positioning System), and preprocessed by being either inserted into a 2.5D grid structure [27,33,36,40,44], or alternatively 3D planes of the buildings' roofs are reconstructed from the point cloud [28,29,31,35,42,45]. Therefore, topological relations are established in order to estimate topographical features such as slope (i.e. inclination) and aspect (i.e. orientation) angles, for accurate calculation of the roofs' solar irradiances. Moreover, with the knowledge of surfaces' characteristics, more accurate shadowing can be performed that significantly reduces the amount of direct irradiance. The calculated solar potential provides a good estimate for the amount of average daily irradiance a given surface receives. However, it does not precisely inform the investors about the predicted production of electrical energy over a given time. In order to solve this problem the efficiency characteristics have to be considered regarding a PVM (photovoltaic module) and the solar inverter connecting PVMs to an electrical grid. One of the solutions is the PV potential metric, which has been a developing topic over the past few years when considering remote sensing data [30,31,41,42,45,46]. PV potential is represented as the integration of reduced instantaneous solar irradiances by considering the nonlinear efficiency characteristics of a given PVM and the solar inverter over a longer period of time. The nonlinearity is inherent from the properties of semiconducting materials that are integral parts of PVMs, and the properties of the MPPT (Maximum Power Point Tracking) technique that is utilized by solar inverters. Most previous works regarding PV potential estimation over urban areas considered these efficiency characteristics as constants, due to lack of measurements for more accurate efficiency modelling. This has led to less accurate estimations, especially in areas with continental climate due to seasonal changes. The constant efficiency characteristics are commonly taken as the average efficiency or a peak efficiency at 1000 Wm^{-2} global irradiance [48], standard air mass AM = 1.5 and temperature $T = 25$ °C. Of course, such efficiency provides only an impression of the nominal power (i.e. overall quality) for a particular PV module or a PV system. However, using constant efficiency characteristic will yield less accurate approximation of the electricity generation, if an accurate location and time-dependent (i.e. spatio-temporal) production of electrical energy is to be estimated that is an integral part of the PV potential metric. Such detailed analysis was already performed on local scale PV systems [49,50], where various surface characteristics were considered. When considering large-scale data, Jakubiec and Reinhart [45] considered first-order approximation in hourly panel efficiency based on ambient air temperature and point irradiation. Strzalka et al. [42] applied a one-diode PV cell model for considering PVM properties. Additionally they considered the consumption ratio on an hourly basis.

This paper presents a novel spatio-temporal PV potential estimation of buildings' roofs that were captured using aerial LiDAR scanning, by considering the nonlinear efficiency characteristics of different types of PVMs, including the solar inverter, and long-term solar irradiance measurements. The nonlinear efficiency characteristics are approximated with irradiance-dependent functions that are modelled from time-series data of irradiance measurements and electrical power. The PV system's instantaneous production of electrical power is estimated by filtering the calculated instantaneous solar irradiance with modelled functions approximating nonlinear efficiency characteristics. Accurate solar irradiance estimation is based on [44] that considers the spatial topographic properties, time-series data of long-term on-site direct and diffuse irradiances that were measured using a pyranometer, and the influence from spatio-temporal multiresolutional shadowing within an urban area from the surrounding terrain and vegetation. The presented method is applicable to any urban area for which LiDAR data and preferably long-term irradiance measurements are available. Furthermore, the method contributes to long-term global PV system development by finding suitable surfaces for PV systems' installation, and forecasting electricity production from different PV modules. The increase of suitably-located PV systems would reduce potential emissions from other energy sources, and assure the return on investments. An extensive comparison between the PVMs' nonlinear and constant efficiency characteristics is performed throughout the entire considered urban area. Moreover, the accuracy of the proposed method is compared with the measurements done by the local power plant located within the scanned urban area.

This paper is structured into four sections. The 2nd section briefly describes previous work on solar irradiance estimation for buildings' roofs using LiDAR data, and presents the newly proposed PV potential, which considers the nonlinear characteristics of the PVM and the solar inverter by nonlinear approximation functions determined by measurements of irradiance and produced electrical power. The analysis for the accuracy of the proposed method, and the comparison between PVMs' constant and nonlinear efficiency characteristics is presented in the Section 3. The Section 4 concludes the paper.

2. Method for estimating photovoltaic potential

The solar potential can generally be defined as the potential suitability of a given surface for a PV system's installation, evaluated by the total [28] or average-daily [44] estimated irradiance the given surface receives throughout the year. In this paper the discussed surface is the rooftop. By going a step further and considering the electrical energy generation by a PV system on a given rooftop, the PV potential can be defined as a metric that provides an accurate prediction of the estimated electrical energy production when using the given PV system throughout the year [30]. Clearly, both solar and PV potentials depend on the underlying irradiance model that is being used. Although one could simply multiply the calculated solar potential by the constant efficiency characteristics, this would only present a rough approximation of the PV potential. Therefore, this paper proposes a new PV potential estimation method over LiDAR data that considers the nonlinear efficiency characteristics of a given PVM type and the solar inverter.

When considering nonlinear efficiency characteristics regarding PV potential, the MPPT (Maximum Power Point Tracking) can be described as a technique of finding such a load connected to the output of a PV cell, PVM or PV array, at which the output power given by the product of output current and voltage, reaches its maximum when considering the given temperature and irradiance [51,52]. The continuously changing load is normally a power electronic device that performs the conditioning of the PV solar cell, module or array, and can be considered as a part of the inverter.

The next two subsections provide a brief overview of the solar irradiance model used in previous work for solar potential estimation over LiDAR data [44]. Subsection 2.3 presents the new PV potential estimation method, whilst Subsection 2.4 provides confirmation of the method for horizontal surfaces.

2.1. Preparation of LiDAR data

In order to calculate accurate irradiances of different surfaces, their geometrical properties have to be considered, such as inclination and orientation, as well the spatio-temporal self-shadowing and shadowing from the surroundings. LiDAR is one of the newer available remote sensing technologies that describe surfaces in great detail. Therefore, it is used in this work for estimating solar irradiance and the PV potential of buildings' roofs more accurately. At first the classified geo-referenced LiDAR point cloud (see Fig. 1a) is inserted into a regular grid structure comprising of equal-sized cells (see Fig. 1b). The number of points n that fall into a given cell C depends on the point cloud's density and the cell's resolution (e.g. 1 m^2 size). The i-th cell's C_i height is determined as $C_{i_z} = \max(p_{1z}, p_{2z}, .., p_{nz});\ \forall\ p_j \in C_i$, where p_j is the height of the j-th point located in the given C_i. Each cell is classified based on points' classes located within the cell. The constructed grid's spatial data-structure provides topology of buildings' roofs, hence topographical features can be extracted, as well as shadowing being performed. Terrain, buildings, and vegetation classes are considered, where the classification of LiDAR data is done by using any state of the art classification methods [28,53,54].

Afterwards, the per-cell instantaneous solar irradiance is estimated and serves as the input for estimating the instantaneous production of electrical power, by considering nonlinear functions approximating the efficiency characteristics of different PVMs and a solar inverter.

2.2. Solar irradiance estimation

The slope $\beta_{C_i} \in [0, \pi/2]$ and aspect $\gamma_{C_i} \in [0, 2\pi]$ angles are extracted for the i-th cell before the solar irradiance is estimated. The cell's normal vector N_{C_i} is calculated by using the best-fitting plane algorithm over the points within a given cell and its non-empty neighbouring cells' points. β_{C_i} is the angle between N_{C_i} and the horizontal plane, whilst γ_{C_i} is the angle between the projected N_{C_i} on the horizontal plane and the direction towards geographical north. The i-th cell's terrestrial spatio-temporal instantaneous solar irradiance I is calculated by considering the diffuse I_d [Wm^{-2}] and direct I_b [Wm^{-2}] irradiances from the measurements:

$$I_{C_i}(t) = I_b(t)R_{b_{C_i}}\left(1 - S_{C_i}(t)\right) + I_d(t)R_{d_{C_i}}\left[\mathrm{Wm}^{-2}\right], \tag{1}$$

where t denotes an instance of time. $R_{b_{C_i}} = \cos(\Theta_{C_i})/\cos(\Theta_{C_{iz}})$ and $R_{d_{C_i}} = \cos^2(\beta_{C_i}/2)$ are the correction factors [55] for I_b and I_d, respectively. β_{C_i} and γ_{C_i} are important when calculating $\{\Theta_{C_i}, \Theta_{C_{iz}}\} \in [0, 1]$. Θ_{C_i} is the cell's angle of incidence, whilst $\Theta_{C_{iz}}$ is the angle of incidence for the horizontal surface (i.e. zenith angle). $S_{C_i}(t) \in [0, 1]$ is the shadowing coefficient that is calculated by using the spatio-temporal multiresolution-based shadowing method introduced in Ref. [44], where $S_{C_i}(t) = 1$ if a given cell is fully shadowed. The used shadowing method additionally considers shadowing from a low-resolution DTM (digital terrain model) representing large-scale surroundings (e.g. mountains and hills), in addition to the high-resolution LiDAR data. A given cell $\boldsymbol{b} = [b_x, b_y, b_z]$ is shadowed by cell $\boldsymbol{a} = [a_x, a_y, a_z]$ if $b_z < a_z - D(\boldsymbol{a}, \boldsymbol{b})\mu$, where $D(\boldsymbol{a}, \boldsymbol{b})$ denotes the Euclidian distance between $\boldsymbol{a}$ and $\boldsymbol{b}$, whilst $\mu = c_z/D(c_x, c_y)$ is the unit change of height, considering the sunbeam's directional vector $\boldsymbol{c} = [c_x, c_y, c_z] = [\mathrm{Sun\_pos}_x - a_x, \mathrm{Sun\_pos}_y - a_y, \mathrm{Sun\_pos}_z - a_z]$ passing between $\boldsymbol{a}$ and $\boldsymbol{b}$. Sun's position for a given location and instance of time is calculated by using the highly precise Solar Positional Algorithm [56] that has an uncertainty of $\sim 0.0003°$ when calculating solar azimuth and altitude angles. Additionally, spatio-temporal transparent shadowing from the vegetation is considered by using LAI (Leaf Area Index) [57], which is variable throughout the year. Light transmission through the vegetation canopies is used to estimate the approximate shadowing coefficient $S_{C_i}(t) = 1 - e^{-K\ \mathrm{LAI}}$ [44]. $K \in [0, 1]$ is the extinction coefficient that depends on solar zenith angle and distribution of the leaves' inclination angles [58]. LAI $\in [0, \infty)$ is the ratio of the canopy's leaves divided by the area of the projected canopy on a horizontal surface. Note that reflected irradiance is excluded as the materials' reflective properties cannot be derived from LiDAR data.

Fig. 2a shows the time-series data of direct and diffuse shortwave irradiances that were obtained by using a pyranometer on horizontal surface at Maribor Edvard Rusjan Airport (46° 28.75′ N, 15° 41.16′ E) in Slovenia. The averaged series of these measurements over 30 min intervals in each day throughout ten years (see Fig. 2b) can serve as the base input in Eq. (1), where the time-dependent I_b and I_d are required. The diffuse irradiance can also be empirically modelled by using a more advanced irradiance model for specific sky conditions (see Demain et al. [17]).

2.3. Estimation of produced electrical energy and the PV potential

This paper considers a single PVM equipped with a micro solar inverter to be placed on each cell C_i within the constructed grid data-structure. The irradiance-dependent efficiency characteristics function $\eta^X_{C_i}(I_{C_i}(t))$ for a given PVM type X over the grid's cell C_i, is approximated as [59]:

$$\eta^X_{C_i}(I_{C_i}(t)) = p_1\left(p_2\left(\frac{I_{C_i}(t)}{1000}\right) + \left(\frac{I_{C_i}(t)}{1000}\right)^{p_3}\right)(2 + p_4 + p_5), \tag{2}$$

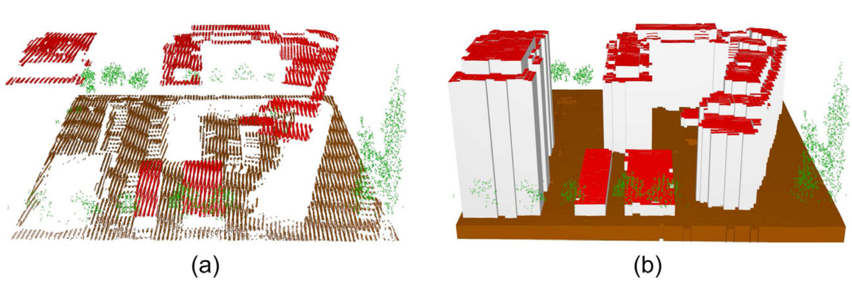

Fig. 1. Visualization of a) classified LiDAR point cloud (terrain, buildings, and vegetation are coloured in brown, red, and green respectively), and b) constructed grid from the point cloud. Vegetation in b) is visualized as point cloud for visual clarity. (For interpretation of the references to colour in this figure legend, the reader is referred to the web version of this article.)

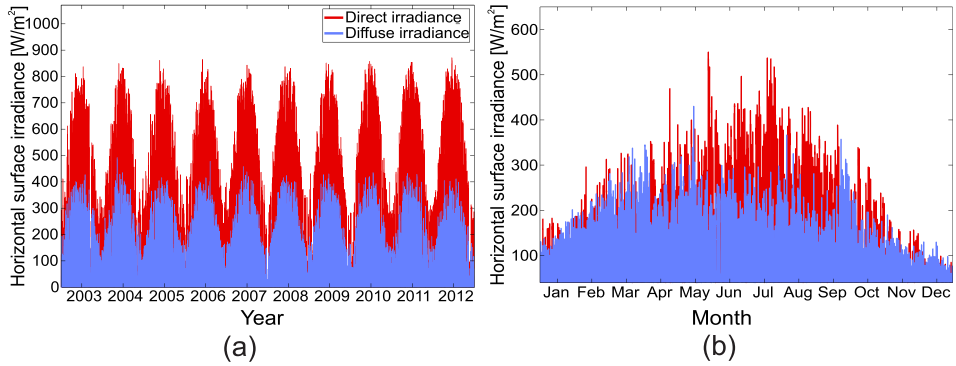

Fig. 2. a) Measured direct and diffuse irradiances by using a pyranometer near Maribor, Slovenia; b) Averaged annual measurements from a) by using a 30 min time-step.

where p_1, p_2, p_3, p_4, and p_5 are the parameters of the efficiency characteristic approximation functions that have to be determined separately for each type of PVM. This form of efficiency characteristics function was proposed by Durisch et al. [59], where the PVM's standard temperature of $T = 25\ ^\circ\mathrm{C}$ and air mass AM = 1.5, but with varying received time-dependent irradiance $I_{C_i}(t)$, are considered. Determination of the nonlinear approximation function's parameters can be achieved by using any optimisation method for nonlinear least square fitting (e.g. linear regression methods for curve fitting). In this paper, the nonlinear efficiency characteristics of the three better known PVMs are considered based on the following semiconductive materials: A-Si (amorphous silicon), P-Si (polycrystalline silicon), and M-Si (monocrystalline silicon). Therefore, the following set of PVMs X = {A-Si, P-Si, M-Si} is considered throughout the rest of the paper. Using time-series data of measurements for each PVM's input irradiance and produced electrical power at the University of Maribor in Slovenia (46° 22.37′ N, 15° 5.91′ E), the functions' parameters were modelled as shown in Table 1. The considered PV modules manufacturers' original data is shown in Appendix A.

Fig. 3a shows the measured data and their approximations using nonlinear functions, by considering the parameters from Table 1. As can be observed in Fig. 3a, the overall efficiency characteristic of M-Si is better than A-Si and P-Si. The time-dependent generated electrical power for a given PV module at cell C_i is calculated as:

$$M_{C_i}^X(I_{C_i}(t)) = \eta_{C_i}^X(I_{C_i}(t))I_{C_i}(t)A_{C_i}[\mathrm{W}], \tag{3}$$

where $A_{C_i}[m^2]$ denotes the area of a given cell C_i, where the cell's inclination β_i is considered (i.e. more inclined surfaces in 2.5D grid have higher areas). The produced electrical power $M_{C_i}^X(I_{C_i}(t))$ is then transferred into PV system's AC power, hence the efficiency characteristic $\eta_{C_i}^{\mathrm{inv}}$ of the per-cell micro solar inverter is considered:

$$P_{C_i}^X(I_{C_i}(t)) = \eta_{C_i}^{\mathrm{inv}}\left(M_{C_i}^X(I_{C_i}(t))\right)M_{C_i}^X(I_{C_i}(t))[\mathrm{W}]. \tag{4}$$

The inverter's efficiency characteristic $\eta_{C_i}^{\mathrm{inv}}(M_{C_i}^X(I_{C_i}(t)))$ was approximated with an exponential function where its parameters were fitted with the aim of reaching the best agreement with the measured efficiency (see Fig. 3b):

$$\eta_{C_i}^{\mathrm{inv}}\left(M_{C_i}^X(I_{C_i}(t))\right) = -0.2871e^{-0.0366\,M_{C_i}^X(I_{C_i}(t))} - 0.6556e^{-0.1575\,M_{C_i}^X(I_{C_i}(t))} + 0.9427. \tag{5}$$

It should be pointed out that $\eta_{C_i}^X(I_{C_i}(t))$ and $\eta_{C_i}^{\mathrm{inv}}(M_{C_i}^X(I_{C_i}(t)))$ were determined by considering MPPT. Although a macro inverter could be used for handling multiple PVMs, the method would be generally less accurate. For example, if multiple PVMs are connected to a macro-inverter, and some PVMs are shadowed, then the entire arrays of PVMs that are connected in series could be blocked. In order to solve this, substantial spatial optimisations would be required when considering various geometrical properties for different roofs.

The overall nonlinear efficiency characteristics of a PV system are shown in Fig. 3c, where PVMs efficiency characteristics are multiplied by η^{inv}. The efficiency degradation by PV modules' ageing is additionally included, by considering the analytical review from Jordan et al. [60]. They calculated the PV module's median degradation rates [%/year] for A-Si, P-Si, and M-Si as 0.87%, 0.64%, and 0.36%, respectively. When considering the PV system with inverter, they calculated the degradation rate for A-Si, P-Si, and M-Si as 0.95%, 0.59%, and 0.23%, respectively (see Fig. 3c). By integrating the instantaneous production of electrical power within the time interval $[t_1, t_2]$, the produced electrical energy is denoted as:

$$E_{C_i}^X(t_1, t_2) = \int_{t_1}^{t_2} \eta_{C_i}^{\mathrm{inv}}\left(M_{C_i}^X(I_{C_i}(t))\right)M_{C_i}^X(I_{C_i}(t))\mathrm{d}t[\mathrm{Wh}]. \tag{6}$$

The proposed per-cell PV potential is then calculated as the average daily produced electrical energy $E_{d_nC_i}^X(\mathrm{sr}_n, \mathrm{ss}_n)$ throughout the year:

$$\overline{E_{dC_i}^X} = \frac{1}{365}\sum_{n=1}^{365} E_{d_nC_i}^X(\mathrm{sr}_n, \mathrm{ss}_n)\left[\mathrm{Whm}^{-2}\right], \tag{7}$$

where sr_n and ss_n denote the sunrise and sunset times for the n-th day in the year. Although the presented nonlinear efficiency characteristics functions were modelled based on the power plant measurements, they can be applied for PV potential modelling over any location, for which LiDAR data is available.

Table 1
Parameters of the nonlinear functions approximating efficiency characteristics for different types of PVMs.

PVM type (X)	p_1	p_2	p_3	p_4	p_5
A-Si	5.5649	−0.7576	0.6601	−3.2976	6.6581
P-Si	4.9009	−0.1770	0.0794	0.0244	1.1248
M-Si	2.3243	−0.2803	0.1783	1.4650	6.2331

2.4. Confirmation of the proposed method for horizontal surfaces

Firstly, the impact of applied efficiency characteristics on the estimated electrical energy production of PVMs placed on a

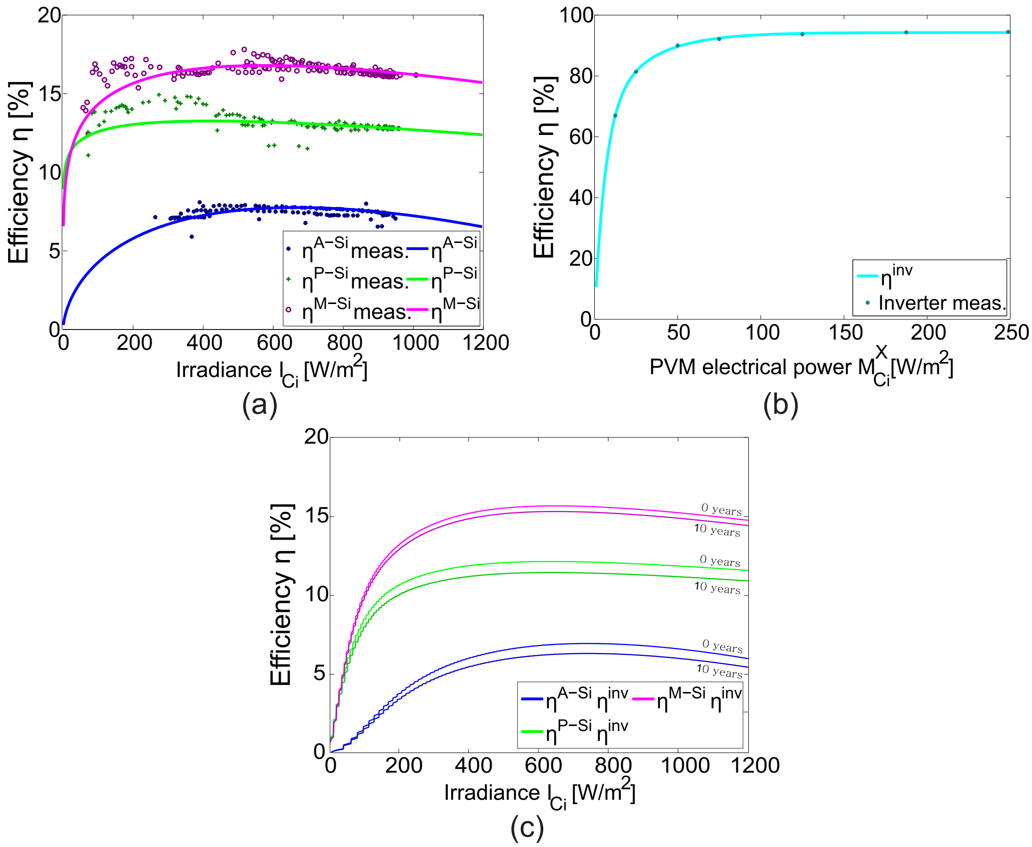

Fig. 3. Nonlinear functions approximating a) the efficiency characteristics of different PVMs, b) a micro solar inverter, c) the PV system's efficiency characteristics, by also considering influence from aging for a duration of 10 years. The dots represent the measured efficiency from hourly irradiances for each material and the solar inverter, throughout the year, whilst the approximation functions are represented by lines.

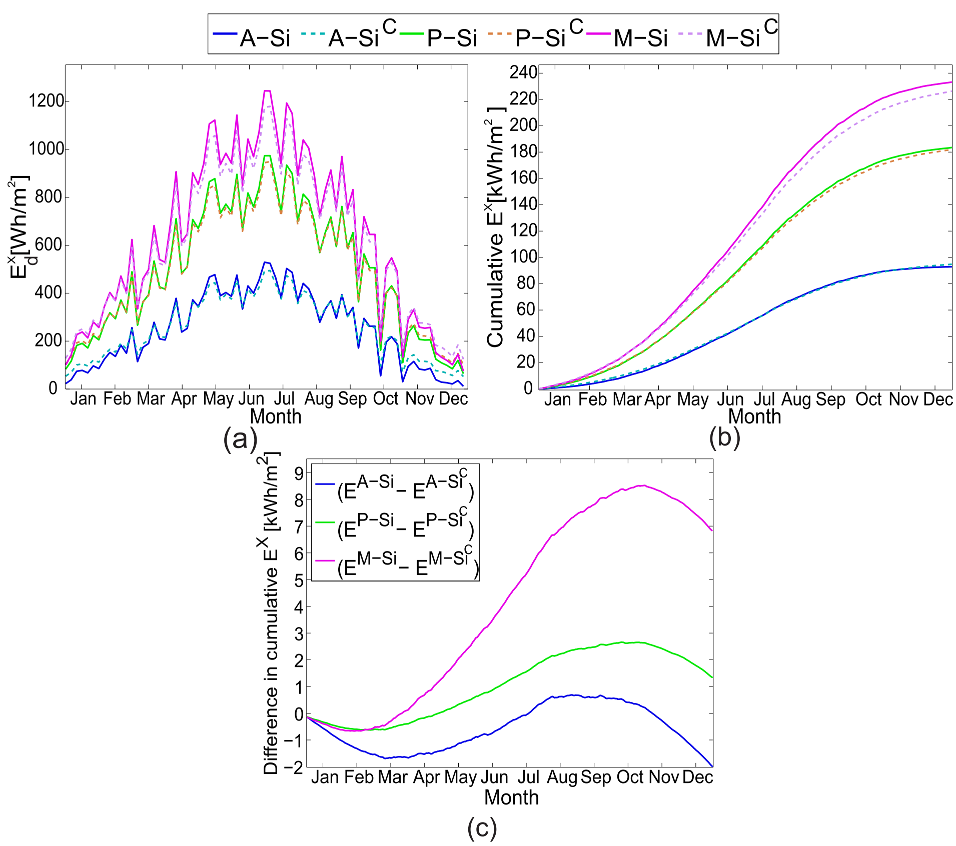

Fig. 4. a) Daily produced electrical energy E_d^X on a horizontal surface throughout the year with 30 min interval; b) cumulative E^x throughout the year; c) cumulative difference in energy production E^x between constant and nonlinear efficiency characteristics.

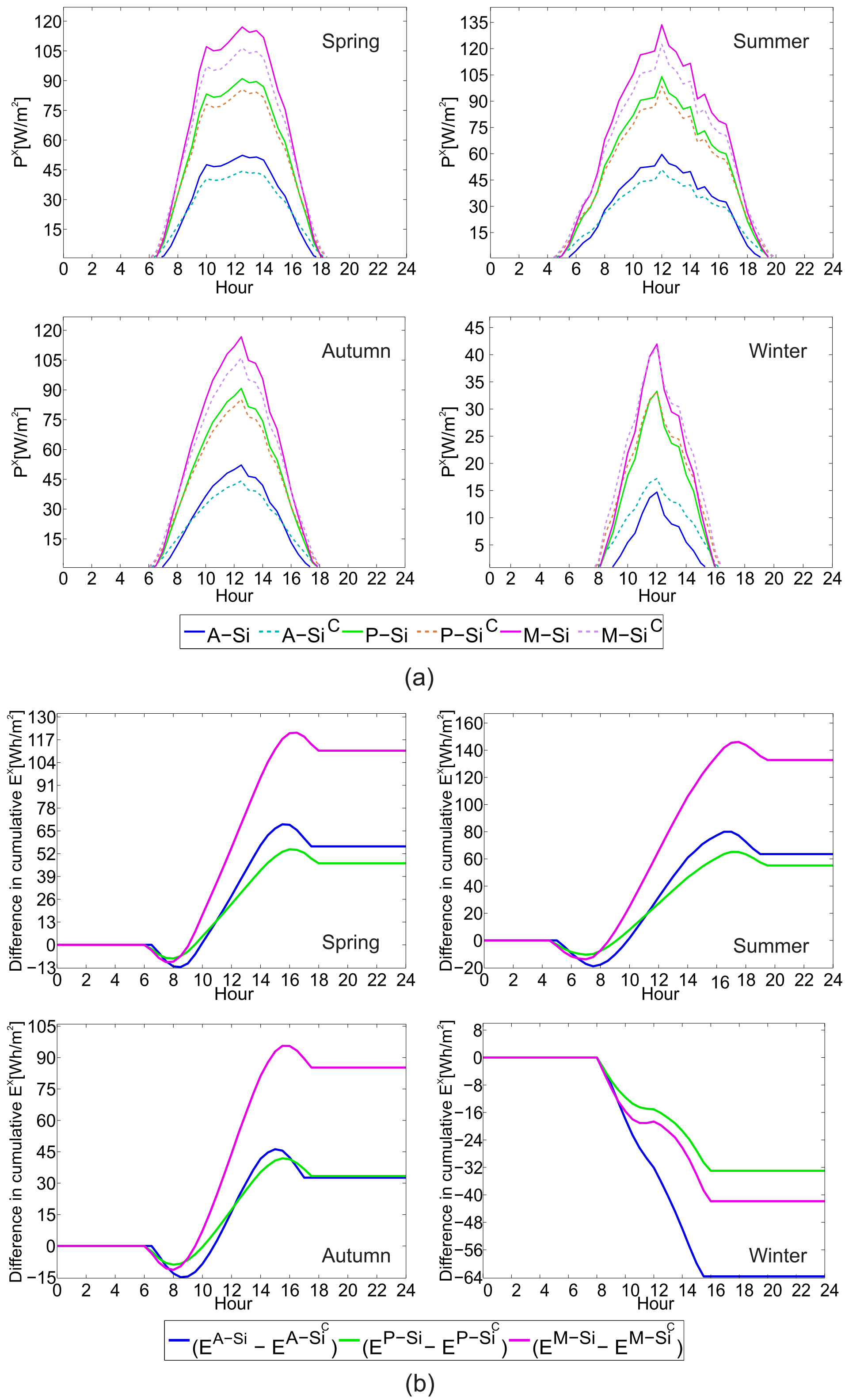

Fig. 5. a) Hourly produced power P^x, during the spring equinox, summer solstice, autumn equinox, and winter solstice; b) cumulative differences in energy production E^x between the PVMs' constant and nonlinear efficiency characteristics throughout the day.

horizontal surface is extensively analysed, in order to confirm the expected discrepancies between constant and nonlinear efficiency characteristics, before applying the method over LiDAR data. The daily produced energy E_d^X for a horizontal surface is shown in Fig. 4a, by considering constant and nonlinear efficiency characteristics for different types of PVMs and the micro solar inverter. The input irradiance measurements on a horizontal surface that are considered in this analysis are shown in Fig. 2b. The

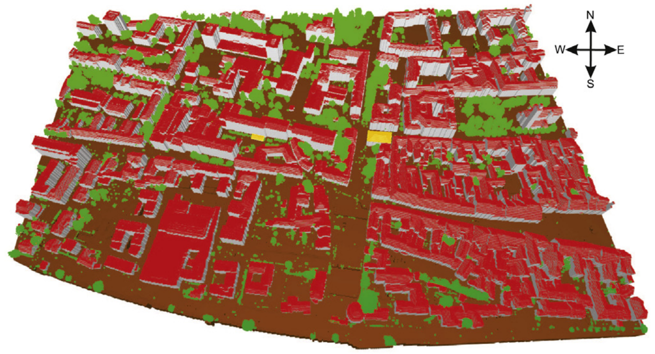

Fig. 6. Visualization of the constructed grid of the considered test site that was obtained with aerial LiDAR scanning. The discussed power plant and the segmented building that were used for further analysis in this section, are marked with yellow rectangles. (For interpretation of the references to colour in this figure legend, the reader is referred to the web version of this article.)

differences between the PVMs constant and nonlinear efficiency characteristics are clearly visible. The PVMs' constant efficiency characteristics are defined as $\eta_{C_i}^{A-Si^C} = 6.7\%$, $\eta_{C_i}^{P-Si^C} = 13\%$, and $\eta_{C_i}^{M-Si^C} = 15.1\%$ for A-Si, P-Si, and M-Si, respectively, where the superscript C denotes constant efficiencies. These are calculated as the averages from the functions approximating the nonlinear efficiency characteristics (see Fig. 3a), where the input global irradiance is considered within the [0, 1200] Wm^{-2} range. Similarly the micro inverter's constant efficiency characteristic is calculated as $\eta_{C_i}^{inv^C} = 89.6\%$. Cumulative energy production E^x throughout the year is shown in Fig. 4b, whilst in Fig. 4c the cumulative differences in energy production E^x can be seen between constant and nonlinear efficiency characteristics. For horizontal surfaces, the nonlinear efficiency characteristic results in a greater cumulative production of electrical power in the cases of P-Si and M-Si (see Fig. 4b, c).

The largest differences between nonlinear and constant efficiency characteristics can be seen during the summer for all three considered PVM types, where an underestimation occurs using the constant efficiency. In contrast, during the winter an overestimation occurs when using the constant efficiency. This is a consequence of using the average value from nonlinear efficiencies for calculating the constant efficiencies. More detailed analysis can be seen in Fig. 5, where a comparison has been done for four example 'extreme' days (i.e. the beginning of each season) of the year, since the given location has continental climate. The cumulative differences in E^x between constant and nonlinear efficiency characteristics are fairly similar during the autumn and spring (see Fig. 5b). During the summer the cumulative difference in produced energy is greater, where an underestimation is achieved when considering constant efficiency. This is caused due to longer daytime, as nonlinear efficiencies are longer relatively close to their peak value. As previously observed, during the winter, a higher energy production is estimated using the constant efficiency characteristics (i.e. overestimation), which is a consequence of low irradiance due to increased overcast and shorter daytimes. Hence, during the winter the nonlinear efficiency characteristics rarely reach the average efficiency.

Moreover, when considering the A-Si^C, a more significant overestimation exists during the winter as opposed to other seasons of the year. This is because A-Si has generally lower efficiency at lower irradiances than the other two considered PVMs, which can be seen in the lower slope of the approximation function (see

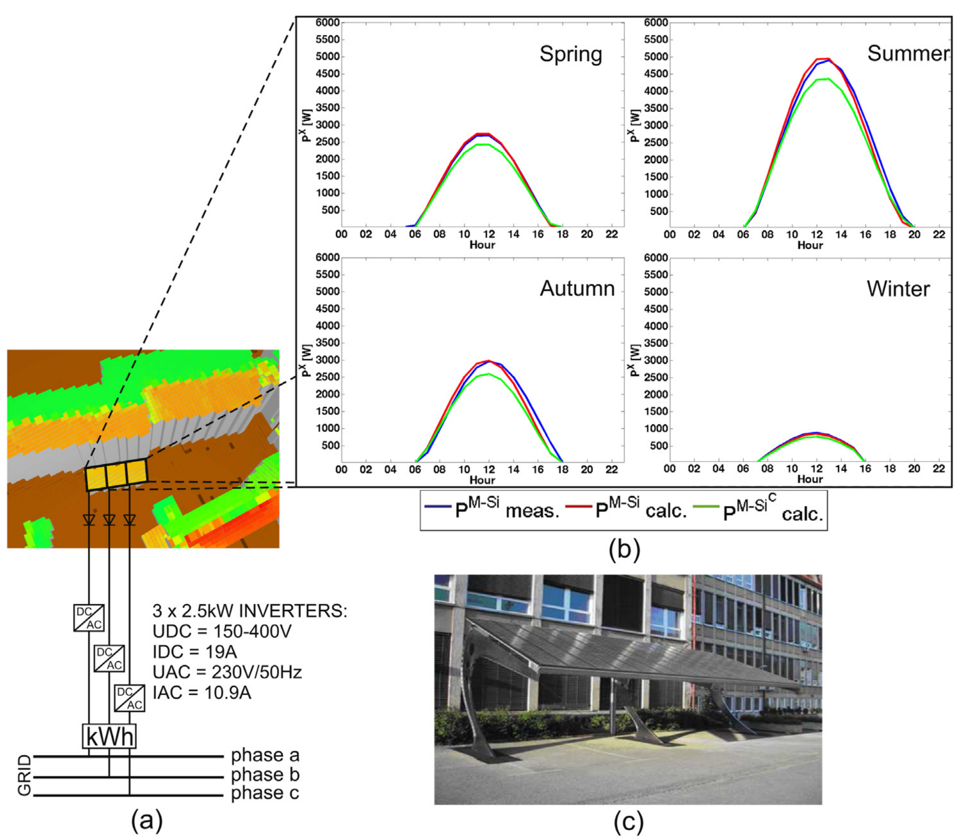

Fig. 7. a) The visualization of FEECS power plant within considered LiDAR data, and the inverters schematic structure; b) Comparison between the onsite measurements done at the power plant with estimated production of electrical power for four extreme days; c) Photograph of the considered power plant.

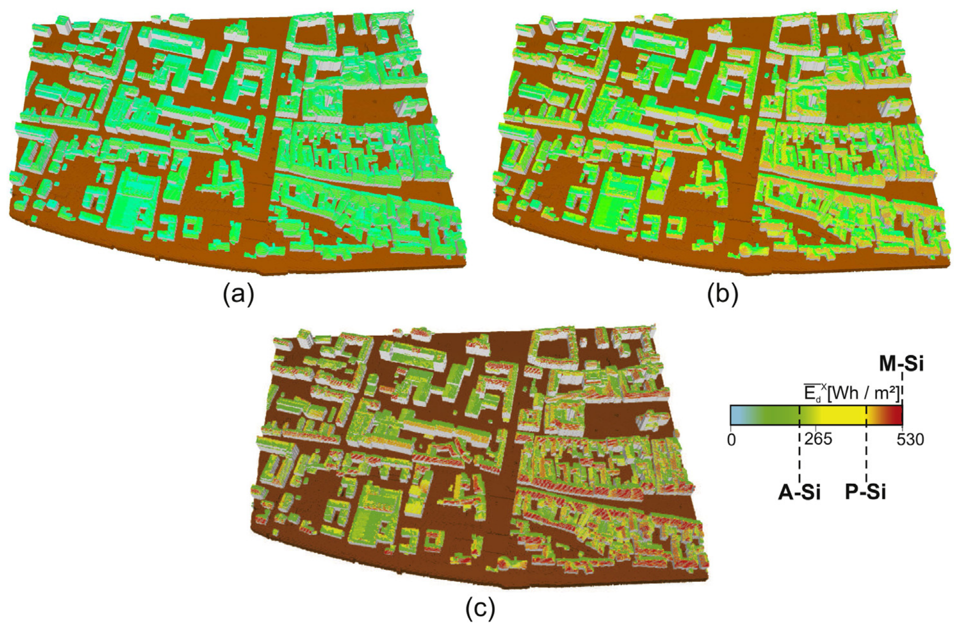

Fig. 8. Calculated PV potential for a) $\overline{E_d}^{A-Si}$, b) $\overline{E_d}^{P-Si}$, and c) $\overline{E_d}^{M-Si}$ (as defined in Equation (7)), PVMs, where the colours of the roofs correspond to the intensity of the PV potential. The vegetation was omitted from the visualization in order to see the buildings' roofs more clearly.

Fig. 3a). The next section shows the efficiency-differences for inclined and oriented roofs' surfaces from real spatial data obtained with aerial LiDAR scanning, where topographical features and influences from shadowing are additionally considered.

3. Results

The proposed method was performed on $\sim$0.5 km^2 urban part (46° 33.5′ N, 15° 38.5′ E) of Maribor city in Slovenia. The classified LiDAR point cloud was inserted into a grid with 1 m^2 per-cell resolution, as can be seen in Fig. 6.

At first, the accuracy of the proposed method was tested by comparing the estimated electrical power with measured production of electrical power obtained by the local 7.5 kWp grid-connected PV power plant at the Faculty of Electrical Engineering and Computer Science (46° 33.54′ N, 15° 38.38′ E) in Maribor (see Fig. 7a, c). The power plant's PV system was equipped with M-Si PVM that is an older type of PVM than the one shown in Table 1. Therefore,

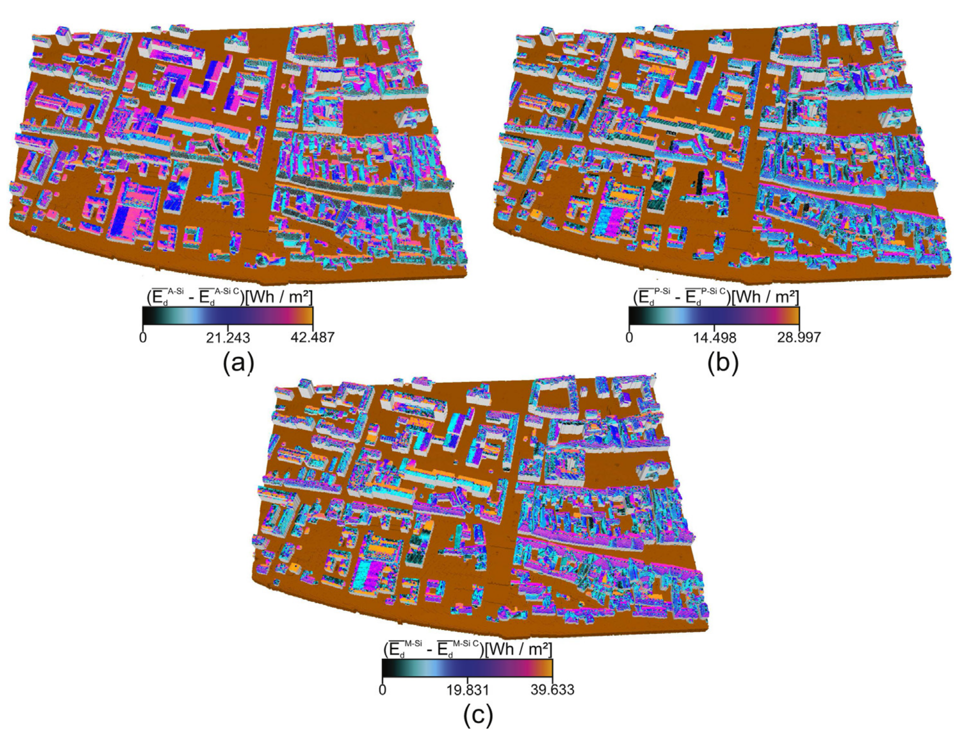

Fig. 9. Differences in estimated PV potential when using constant and nonlinear efficiency characteristics for the micro solar inverter and different PVMs: a) $\overline{E_d}^{A-Si}$, b) $\overline{E_d}^{P-Si}$, and c) $\overline{E_d}^{M-Si}$.

its nonlinear efficiency approximated function fitting parameters were calculated as $p_1 = 2.922$, $p_2 = 0.44919$, $p_3 = 0.30913$, $p_4 = 2.67053$, and $p_5 = 1.95004$. The plant's time-series data of measured produced power was available for the duration of 2006–2012 with a 5 min time-step, which were then averaged over a 30 min interval in order to estimate an average-year from the duration of 6 years of measurements. The averaged measured data was then compared with the predicted electrical power by using the proposed method and applying the same time-step.

Three 2.5 kW inverters were operating at the local power plant (see Fig. 7a). Therefore in order to achieve a more accurate comparison, the power plant was spatially divided into three equally-large regions, each for one inverter (see Fig. 7a). As the measurements were available for the 2.5 kW inverter, its efficiency was approximated using:

$$\eta_r^{\mathrm{inv}}\left(M_r^{\mathrm{M-Si}}(I_r)\right) = -0.7965e^{-0.0231\,M_r^{\mathrm{M-Si}}(I_r)} - 0.0874e^{-0.0006\,M_r^{\mathrm{M-Si}}(I_r)} + 0.9377, \qquad (8)$$

where $M_r^{\mathrm{M-Si}}(I_r) = \sum_{i=1}^{m} M_{C_i}^{\mathrm{M-Si}}(I_{C_i}), C_i \in r$, and r defines one of the three regions with its own inverter. Each region consisted of m cells (i.e. PVMs) with well-defined connections, which sufficed for validation purposes. The estimated total electrical power was then calculated as $P^{\mathrm{M-Si}}(M_r^{\mathrm{M-Si}}(I_r)) = \sum_{r=1}^{3} \eta_r^{\mathrm{inv}}(M_r^{\mathrm{M-Si}}(I_r))M_r^{\mathrm{M-Si}}(I_r)$. Since multiple PVMs were connected to each inverter, the calculated shadowing played a key role in the accuracy of the proposed method. Fig. 7b shows the comparison between the estimated produced power and the measured production over four extreme days. In the autumn and the spring, the nonlinear efficiency characteristics had an overestimation of 2% in comparison with the measured produced electricity, whilst when considering the constant efficiency characteristics an underestimation of 10% occurred. During the summer the nonlinear efficiency had an overestimation of 1%, and the constant efficiency an underestimation of 8%. During the winter, the nonlinear and constant efficiency characteristics had underestimations of 4% and 12%, respectively.

Over the considered area (as shown in Fig. 6) the proposed PV potential was estimated by using the nonlinear efficiency characteristics of different PVMs and the solar micro-inverter, as can be seen in Fig. 8. M-Si PVM type had a maximum PV potential of 530 [$\mathrm{Whm^{-2}}$] and was the most efficient of all three considered PVMs used within the considered urban area. M-Si and A-Si had maximum PV potentials of 418 [$\mathrm{Whm^{-2}}$] and 210 [$\mathrm{Whm^{-2}}$], respectively. When calculating the spatio-temporal irradiance for PV potential, the time-dependent direct and diffuse solar irradiances were considered that were based on 10 years of measurements (as shown earlier in Fig. 2b) with 30 min time-steps.

Further analysis was performed by calculating the difference between the buildings' roofs PV potential when considering constant and nonlinear efficiency characteristics regarding different PVMs and a solar inverter. This was done per-cell, as shown in Fig. 9. The largest difference can be seen in A-Si$^{\mathrm{C}}$, where the maximum difference of 42.5 [$\mathrm{Whm^{-2}}$] corresponded to a difference of 20.2% (i.e. 42.5/210), whilst the maximum differences for P-Si and M-Si were 29.0 and 39.6 [$\mathrm{Whm^{-2}}$], respectively. This corresponded to 6.9% and 7.5% differences in estimation (i.e. underestimation), respectively. Furthermore, in all three cases, the least differences were found for roofs oriented toward the south, whilst the highest differences occurred when considering flat roofs with negligible inclinations. Roofs oriented towards the north had similar differences when considering P-Si$^{\mathrm{C}}$ or M-Si$^{\mathrm{C}}$, whilst being almost equal as in the cases of flat roofs when considering A-Si$^{\mathrm{C}}$.

The degradation of the PV systems' due to ageing was also analysed. This was done by calculating the difference in cumulative electrical energy production for the next 10 years with and without considering the influence of ageing. In Fig. 10 the calculated differences can be seen, where the least difference was observed in the case of M-Si, and the largest for P-Si. The differences for M-Si and P-Si appear consistent within the spatial-temporal context,

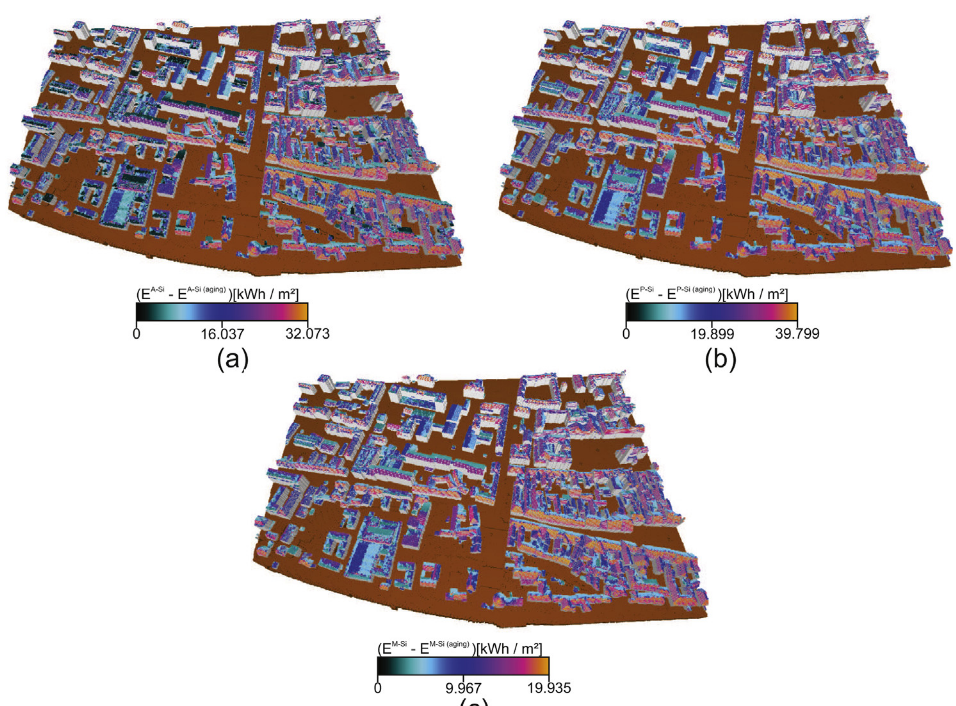

Fig. 10. Differences in cumulative estimated electrical energy production with and without using the influence of aging for the next 10 years, when considering different PVMs: a) $E^{\mathrm{A-Si}}$, b) $E^{\mathrm{P-Si}}$, and c) $E^{\mathrm{M-Si}}$.

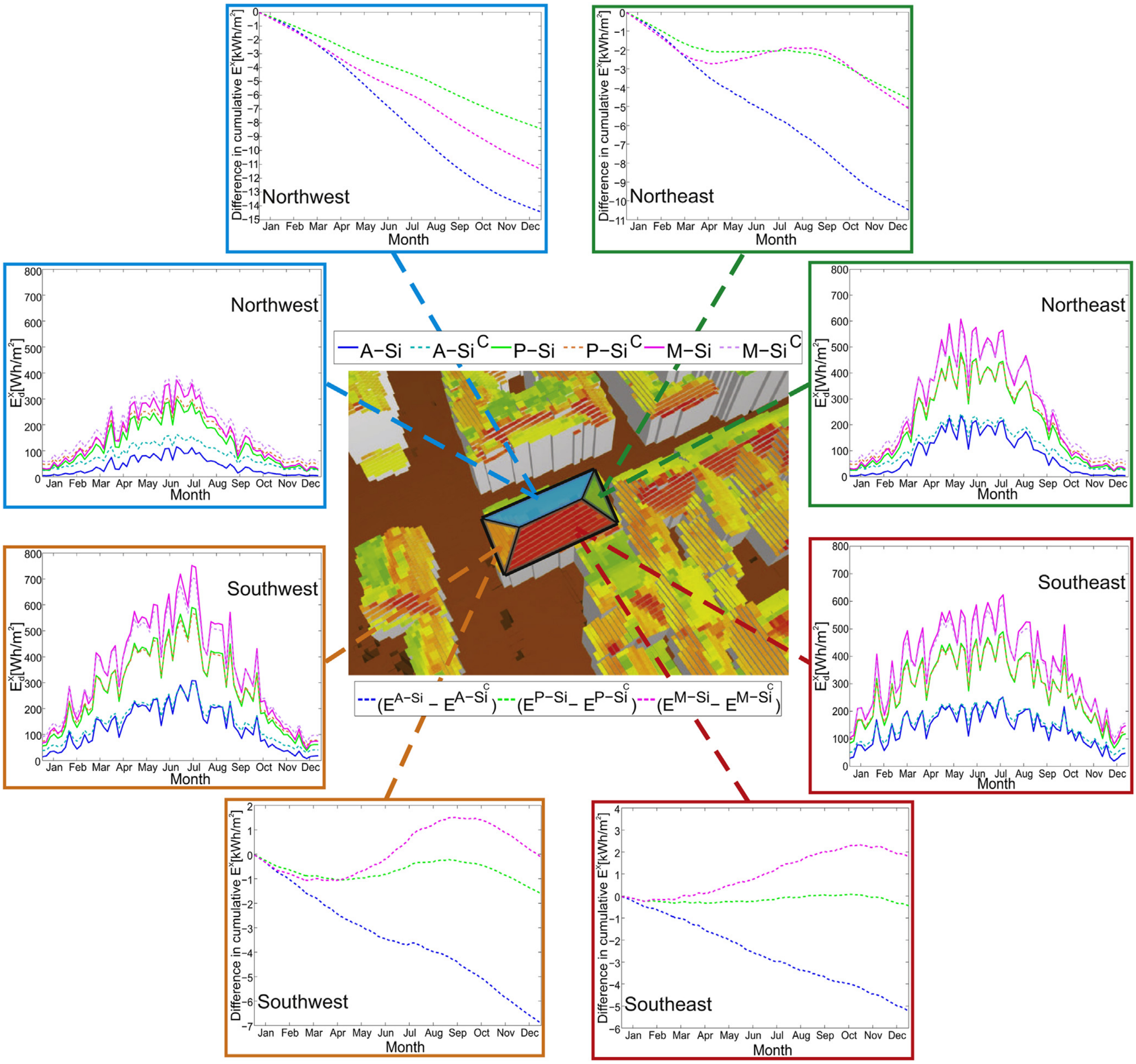

Fig. 11. Segments' average cell's $E^X_{dC_i}$, by considering building roofs' segments oriented northeast, southeast, northwest, and southwest. Two corresponding graphs are shown for each segment: produced electrical energy throughout the year when using different efficiency characteristics, and cumulative differences between constant and nonlinear efficiency characteristics.

where the largest differences occurred for roofs oriented towards the south. Although similar results were observed for A-Si, the horizontal and north-oriented surfaces had slightly higher differences.

In order to see the discussed efficiency-difference in spatial context, additional analyses were performed on four different roofs' segments that were oriented towards the four ordinal geographical directions, as shown in Fig. 11. The average per-cell daily produced electrical energy $E^X_{dC_i}$ was calculated for each roof. The roof's segmentation was performed by the algorithm that was previously used in Ref. [44]. In all four cases the highest overestimation in cumulative $E^X_{dC_i}$ occurred when considering A-Si^C, as previously observed in Fig. 9a. Moreover, the roofs oriented towards the south had lower underestimations when considering M-Si^C and P-Si^C, as opposed to north-oriented roofs where all three considered PVMs had more significant overestimations with constant efficiency characteristics.

4. Conclusion

This paper proposed a novel method for calculating PV (photovoltaic) potential by estimating average daily production of electrical energy throughout the year, over LiDAR (Light Detection And Ranging) data. The estimation of produced electrical power was done by considering nonlinear efficiency characteristics for different types of PVMs (photovoltaic modules) and a solar micro-inverter. These were approximated with modelled irradiance-dependent functions that were best-fitted to the measured electrical power in order to approximate efficiency characteristics. This was achieved with an efficiency model for each type of considered semiconducting material used in PVMs. The presented method also takes into account the efficiency degradation of PVM modules with regard to their age. The estimation's input was the accurately calculated per-cell solar irradiance with a given time-step, where different influential factors were considered (e.g. topography, self-shadowing, vegetation and shadowing from the surrounding terrains together with long-term time-series data of direct and diffuse solar irradiance measurements).

To our knowledge, the presented method is the first that uses the nonlinear efficiency characteristics of multiple PVMs and a solar inverter, when estimating PV potential over buildings' roofs obtained with ALS (aerial laser scanning), and long-term irradiance measurements. However, this method is also applicable to geospatial 3D data acquired from other remote sensing technologies. When considering constant efficiency characteristics several estimation errors regarding the predicted production of electrical power were shown within a spatio-temporal context, since they were calculated as the average values from functions approximating nonlinear efficiency characteristics. Moreover, the presented method has high accuracy as was shown in the comparison with the measurements at the local solar power plant. The accuracy mainly depends on the resolution of the input data (e.g. LiDAR point cloud and irradiance measurements) of the presented method. With this work, more accurate insights are provided for solar energy investments within large-scale urban areas. For future-work, a higher accuracy would be achieved by considering spatio-temporal influence of temperature and air mass at the PVM level.

Acknowledgements

Thanks to GEOIN d.o.o. (in Maribor; Slovenia) for providing the classified LiDAR datasets, and to the Slovenian Environment Agency for the measurements done with the pyranometer. This work was supported by Slovenian Research Agency under research contracts 1000-13-0552, J2-5479, P2-0041, L2-5489, L2-4114, and P2-0115.

Appendix A

Table A.1
Manufacturer's original data for the considered PV module types.

Manufacturer's original data	PV module		
	A-Si	P-Si	M-Si
Efficiency	7.4%	12.9%	15.9%
Nominal power	77 W	233 W	190 W
Deviation in power	±5%	±3%	±3%
Short-circuit current	1.2 A	8.5 A	5.6 A
Maximum power point voltage	69.9 V	29.3 V	36.7 V
Nominal operating cell temperature	45 °C	44 °C	72 °C

References

[1] Lewis NS. Toward cost-effective solar energy use. Science 2007;315(5813):798–801.
[2] Eltawil MA, Zhao Z. Grid-connected photovoltaic power systems: technical and potential problems – A review. Renew Sustain Energy Rev 2010;14(1):112–29.
[3] Singh GK. Solar power generation by PV (photovoltaic) technology: a review. Energy 2003;53:1–13.
[4] Bugler JW. The determination of hourly insolation on an inclined plane using a diffuse irradiance model based on hourly measured global horizontal insolation. Sol Energy 1977;19(5):477–91.
[5] Willmot CJ. On the climatic optimization of the tilt and azimuth of flat-plate solar collectors. Sol Energy 1982;28(3):205–16.
[6] Perez R, Seals R, Ineichen P, Stewart R, Menicucci D. A new simplified version of the perez diffuse irradiance model for tilted surfaces. Sol Energy 1987;39(3):221–31.
[7] Perez R, Ineichen P, Moore K, Kmiecik M, Chain C, George R, et al. A new operational model for satellite-derived irradiances: description and validation. Sol Energy 2002;73(5):307–17.
[8] Robinson D, Stone A. Solar radiation modelling in the urban context 2004. Sol energy 2004;77(3):295–309.
[9] Šúri M, Hofierka J. A new GIS-based solar radiation model and its application to photovoltaic assessments. Trans GIS 2004;8(2):175–90.
[10] Arboit M, Diblasi A, Fernández Llano JC, De Rosa C. Assessing the solar potential of low-density urban environments in Andean cities with desert climates: the case of the city of Mendoza, in Argentina. Renew Energy 2008;33(8):1733–48.
[11] Pandey CK, Katiyar AK. A note on diffuse solar radiation on a tilted surface. Energy 2009;34(11):1764–9.
[12] Tapiador FJ. Assessment of renewable energy potential through satellite data and numerical models. Energy Environ Sci 2009;11:1142–61.
[13] Coskun C, Oktay Z, Dincer I. Estimation of monthly solar radiation distribution for solar energy system analysis. Energy 2011;3(2):1319–23.
[14] Linares-Rodríguez A, Ruiz-Arias JA, Pozo-Vázquez D, Tovar-Pescador J. Generation of synthetic daily global solar radiation data based on ERA-interim reanalysis and artificial neural networks. Energy 2011;36(8):5356–65.
[15] Li H, Bu X, Long Z, Zhao L, Ma W. Calculating the diffuse solar radiation in regions without solar radiation measurements. Energy 2012;44(1):611–5.
[16] Notton G, Paoli C, Vasileva S, Nivet ML, Canaletti JL, Cristofari C. Estimation of hourly global solar irradiation on tilted planes from horizontal one using artificial neural networks. Energy 2012;39(1):166–79.
[17] Demain C, Journée M, Bertrand C. Evaluation of different models to estimate the global solar radiation on inclined surfaces. Renew Energy 2013;50:710–21.
[18] Khalil SA, Shaffie AM. A comparative study of total, direct and diffuse solar irradiance by using different models on horizontal and inclined surfaces for Cairo, Egypt. Renew Sustain Energy Rev 2013;27:853–63.
[19] Li DH, Chau NT, Wan KK. Predicting daylight illuminance and solar irradiance on vertical surfaces based on classified standard skies. Energy 2013;53:252–8.
[20] Aste N, Del Pero C, Leonforte F, Manfren M. A simplified model for the estimation of energy production of PV systems. Energy 2013;59:503–12.
[21] Khorasanizadeh H, Mohammadi K. Introducing the best model for predicting the monthly mean global solar radiation over six major cities of Iran. Energy 2013;51(1):257–66.
[22] Kisi O. Modeling solar radiation of Mediterranean region in Turkey by using fuzzy genetic approach. Energy 2014;64:429–36.
[23] Linares-Rodriguez A, Ruiz-Arias JA, Pozo-Vazquez D, Tovar-Pescador J. An artificial neural network ensemble model for estimating global solar radiation from Meteosat satellite images. Energy 2013;61:636–45.
[24] Moradi I, Mueller R, Perez R. Retrieving daily global solar radiation from routine climate variables. Theor Appl Climatol 2013:1–9.
[25] Petrie G, Toth CK. Airborne and spaceborne laser profilers and scanners. In: Shan J, Toth CK, editors. Topographic laser ranging and scanning: principles and processing. CRC Press; 2008. pp. 29–86.
[26] Izquierdo S, Rodrigues M, Fueyo N. A method for estimating the geographical distribution of the available roof surface area for large-scale photovoltaic energy-potential evaluations. Sol Energy 2008;82(10):929–39.
[27] Yu B, Liu H, Wu J, Lin WM. Investigating impacts of urban morphology on spatio-temporal variations of solar radiation with airborne LIDAR data and a solar flux model: a case study of downtown Houston. Int J Remote Sens 2009;30(17):4359–85.
[28] Jochem A, Höfle B, Rutzinger M, Pfeifer N. Automatic roof plane detection and analysis in airborne lidar. Sensors 2009;9(7):5241–62.
[29] Levinson R, Akbari H, Pomerantz M, Gupta S. Solar access of residential rooftops in four California cities. Sol Energy 2009;83(12):2120–35.
[30] Hofierka J, Kaňuk J. Assessment of photovoltaic potential in urban areas using open-source solar radiation tools. Renew Energy 2009;34(10):2206–14.
[31] Wiginton LK, Nguyen HT, Pearce JM. Quantifying rooftop solar photovoltaic potential for regional renewable energy policy. Comput Environ Urban Syst 2010;34(4):345–57.
[32] Şenkal O. Modeling of solar radiation using remote sensing and artificial neural network in Turkey. Energy 2010;35(12):4795–801.
[33] Tooke TR, Coops NC, Voogt JA, Meitner MJ. Tree structure influences on rooftop-received solar radiation. Landsc Urban Plan 2011;102(2):73–81.
[34] Bergamasco L, Asinari P. Scalable methodology for the photovoltaic solar energy potential assessment based on available roof surface area: application to Piedmont Region (Italy). Sol Energy 2011;85(5):1041–55.
[35] Jochem A, Höfle B, Rutzinger M. Extraction of vertical walls from mobile laser scanning data for solar potential assessment. Remote Sens 2011;3(4):650–67.
[36] Tooke TR, Coops NC, Christen A, Gurtuna O, Prévot A. Integrated irradiance modelling in the urban environment based on remotely sensed data. Sol Energy 2012;86(10):2923–34.
[37] Hofierka J, Zlocha M. A new 3-D solar radiation model for 3-D city models. Trans GIS 2012;16(5):681–90.
[38] Redweik P, Catita C, Brito M. Solar energy potential on roofs and facades in an urban landscape. Sol Energy 2013;97:332–41.
[39] Nguyen HT, Pearce JM, Harrap R, Barger G. The application of LiDAR to assessment of rooftop solar photovoltaic deployment potential in a municipal district unit. Sensors 2012;12(4):4534–58.
[40] Nguyen HT, Pearce JM. Incorporating shading losses in solar photovoltaic potential assessment at the municipal scale. Sol Energy 2012;86(5):1245–60.

[41] Brito MC, Gomes N, Santos T, Tenedório JA. Photovoltaic potential in a Lisbon suburb using LiDAR data. Sol Energy 2012;86(1):283–8.
[42] Strzalka A, Alam N, Duminil E, Coors V, Eicker U. Large scale integration of photovoltaics in cities. Appl Energy 2012;93:413–21.
[43] Ruiz-Arias JA, Terrados J, Pérez-Higueras P, Pozo-Vázquez D, Almonacid G. Assessment of the renewable energies potential for intensive electricity production in the province of Jaén, southern Spain. Renew Sustain Energy Rev 2012;16(5):2994–3001.
[44] Lukač N, Žlaus D, Seme S, Žalik B, Štumberger G. Rating of roofs' surfaces regarding their solar potential and suitability for PV systems, based on LiDAR data. Appl Energy 2013;102:803–12.
[45] Jakubiec JA, Reinhart CF. A method for predicting city-wide electricity gains from photovoltaic panels based on LiDAR and GIS data combined with hourly daysim simulations. Sol Energy 2013;93:127–43.
[46] Nguyen HT, Pearce JM. Automated quantification of solar photovoltaic potential in cities. IRSPSD International 2013;1(1):57–70.
[47] Kucuksari S, Khaleghi AM, Hamidi M, Zhang Y, Szidarovszky F, Bayraksan G, et al. An integrated GIS, optimization and simulation framework for optimal PV size and location in campus area environments. Appl Energy 2014;113:1601–13.
[48] Green MA, Emery K, Hishikawa Y, Warta W, Dunlop ED. Solar cell efficiency tables (version 39). Prog Photovoltaics Res Appl 2012;20(1):12–20.
[49] Notton G, Lazarov V, Stoyanov L. Optimal sizing of a grid-connected PV system for various PV module technologies and inclinations, inverter efficiency characteristics and locations. Renew Energy 2010;35(2):541–54.
[50] Lam KH, Lai TM, Lo WC, To WM. The application of dynamic modelling techniques to the grid-connected PV (photovoltaic) systems. Energy 2012;46(1):264–74.
[51] Hohm DP, Ropp ME. Comparative study of maximum power point tracking algorithms. Prog Photovoltaics Res Appl 2003;11(1):47–62.
[52] Esram T, Chapman PL. Comparison of photovoltaic array maximum power point tracking techniques. IEEE Trans Energy Convers 2007;22(2):439–49.
[53] Heinzel J, Koch B. Exploring full-waveform LiDAR parameters for tree species classification. Int J Appl Earth Obs Geoinform 2011;13(1):152–60.
[54] Mongus D, Žalik B. Parameter-free ground filtering of LiDAR data for automatic DTM generation. ISPRS J Photogramm Remote Sens 2012;67:1–12.
[55] Duffie JA, Beckman WA. Solar engineering of thermal processes. Wiley-Interscience; 2006.
[56] Reda I, Andreas A. Solar position algorithm for solar radiation applications. Sol Energy 2004;76(5):577–89.
[57] Yuan H, Dai Y, Xiao Z, Ji D, Shangguan W. Reprocessing the MODIS leaf area index products for land surface and climate modelling. Remote Sens Environ 2011;115(5):1171–87.
[58] Sinoquet H, Stephan J, Sanohat G, Lauri PE, Monney P. Simple equations to estimate light interception by isolated trees from canopy structure features: assessment with three-dimensional digitized apple trees. New Phytol 2007;175(1):94–106.
[59] Durisch W, Bitnar B, Mayor J, Kiess H, Lam K, Close J. Efficiency model for photovoltaic modules and demonstration of its application to energy yield estimation. Sol Energy Mater Sol Cells 2007;91(1):79–84.
[60] Jordan DC, Kurtz SR. Photovoltaic degradation rates – an analytical review. Prog Photovoltaics Res Appl 2013;21(1):12–29.